



Increased optical pathlength through aqueous media for the infrared microanalysis of live cells

James Doherty^{1,2,3} · Zhe Zhang^{1,2} · Katia Wehbe³ · Gianfelice Cinque³ · Peter Gardner^{1,2} · Joanna Denbigh⁴ 

Received: 8 March 2018 / Revised: 25 May 2018 / Accepted: 6 June 2018 / Published online: 2 July 2018
© The Author(s) 2018

Abstract

The study of live cells using Fourier transform infrared spectroscopy (FTIR) and FTIR microspectroscopy (FT-IRMS) intrinsically yields more information about cell metabolism than comparable experiments using dried or chemically fixed samples. There are, however, a number of barriers to obtaining high-quality vibrational spectra of live cells, including correction for the significant contributions of water bands to the spectra, and the physical stresses placed upon cells by compression in short pathlength sample holders. In this study, we present a water correction method that is able to result in good-quality cell spectra from water layers of 10 and 12 μm and demonstrate that sufficient biological detail is retained to separate spectra of live cells based upon their exposure to different novel anti-cancer agents. The IR brilliance of a synchrotron radiation (SR) source overcomes the problem of the strong water absorption and provides cell spectra with good signal-to-noise ratio for further analysis. Supervised multivariate analysis (MVA) and investigation of average spectra have shown significant separation between control cells and cells treated with the DNA cross-linker PL63 on the basis of phosphate and DNA-related signatures. Meanwhile, the same control cells can be significantly distinguished from cells treated with the protein kinase inhibitor YA1 based on changes in the amide II region. Each of these separations can be linked directly to the known biochemical mode of action of each agent.

Keywords Synchrotron radiation (SR) · Fourier transform infrared spectroscopy (FTIR) · Infrared microspectroscopy (IRMS) · Cancer · Single cell · Drug-cell interactions

Introduction

The use of Fourier transform infrared spectroscopy (FTIR) for the study of biological materials such as tissue, cells, plasma and serum is well established. Infrared (IR) spectra of

biological materials have been used to obtain diagnostic and prognostic information on a range of diseases [1–7], as well as for the study of the effectiveness and mode of action of novel treatments [8–10]. Cancer has been a particular focus, with FTIR explored as a means to both improve diagnosis and inform the design of new treatments.

A significant body of work has demonstrated the ability of IR spectra to provide information on the mode of action of novel chemotherapy agents and assess their effectiveness against different cancer cells [11–13]. Additional work has also investigated drug-resistant cell lines and examined the effects of cell cycle on the uptake of certain drugs [14, 15].

Historically, the majority of cell studies using FTIR have relied on chemically fixed, dried samples. The benefits of this are clear; samples can be easily handled post fixation, and the same sample can be returned to multiple times for repeat measurement, given that IR is a non-destructive method of investigation.

However, chemical fixatives have been shown to have an effect on various structures within the cell, limiting the

✉ Joanna Denbigh
j.l.denbigh@salford.ac.uk

✉ Peter Gardner
peter.gardner@manchester.ac.uk

¹ Manchester Institute of Biotechnology, University of Manchester, 131 Princess Street, Manchester M1 7DN, UK

² School of Chemical Engineering and Analytical Science, University of Manchester, Oxford Road, Manchester M13 9PL, UK

³ Diamond Light Source, Diamond House, Harwell Science and Innovation Campus, Didcot, Oxfordshire OX11 0DE, UK

⁴ Biomedical Research Centre, School of Environment and Life Sciences, University of Salford, Salford M5 4WT, UK

interpretation of resulting spectra [16–18]. Studies of sample dehydration also note changes in peak position, intensity and ratio across the spectrum [19–21]. Cell dehydration can particularly affect DNA bands, with the broader, weaker A-form DNA bands being more prevalent in dehydrated cell spectra, making DNA signatures harder to separate from other spectral contributions from proteins, RNA and carbohydrates [22, 23]. While the biochemical nature of the cell may be broadly maintained, subtle differences within a sample or as a result of stimuli may be lost. Studies of living cells have been able to yield biological and morphological details that were not accessible using fixed samples, particularly when combined with the brilliance of synchrotron radiation (SR) as a source [24–28].

The requirement of an aqueous environment to maintain cell viability is a significant constraint to FTIR analysis of live cells. This introduces the strong absorbance pattern of water into the spectrum in the ~ 1650 and $3000\text{--}3500\text{ cm}^{-1}$ wavenumber ranges, due to OH bending and stretching modes, respectively, which obscures much of the cell spectrum and makes extraction of biochemical information extremely difficult [29].

The water spectrum is a problem for analysts for two primary reasons: (1) the strength of the water absorptions causes insufficient light to penetrate to the sample, giving a signal that is too low to obtain quality data, and (2) the position of the water absorption signatures obscures key biological information relating to the amide and lipid bands arising from cellular species [30, 31].

Some work using living cells in aqueous environments has simply ignored the spectral regions most affected by water [32], but this is clearly severely limiting due to the significant amount of biochemical information being lost.

The removal of water from the acquired spectrum is a non-trivial issue. The subtraction of a pure water spectrum is not ideal, as the spectrum of separate bulk water will be different from that of water interacting with a biological system [33]. Likewise, removing the entire water contribution from the spectrum is also imperfect, as structural water accounts for approximately 70% of the mass of an average cell [34]. A number of water correction methods have been proposed, but with a lack of consensus over a single preferable method.

One method, published by Vaccari and colleagues [18, 35], removes a scaled water spectrum, in which the scaling factor is determined by an algorithm that optimises baseline flatness in the $1800\text{--}2500\text{ cm}^{-1}$ region, which contains no biochemical information but does contain the water combination band. The region containing the water combination band can, however, be heavily influenced by baseline variations.

Quaroni et al. were able to track a range of cellular metabolites by taking a reference spectrum through a cell-free area of growth medium, removing a fraction of the water contribution by a ratio to the background taken through an empty sample holder and then analysing the IR images in second

derivative in order to highlight small spectral changes [36]. However, this does not take into account the different quantities of water present across the field of view of several cells and is therefore prone to under-/over-correcting for the bulk water contribution.

In separate work, Gelfand et al. [37] attempt to account for this over-correction by iteratively re-adding water contributions to their corrected spectra until the differences in baseline on either side of the C-H alkyl stretch at 2900 cm^{-1} was minimised. However, this work relied on a spacer of just $4\text{ }\mu\text{m}$, which is a significant compression for the majority of cells, thereby likely to be picking up biochemical changes due to cellular stress and not mode of action of drug alone.

Deuterated water (D_2O) has been proposed by some as a possible alternative medium to remove the water problem, due to its similar physical properties but significantly shifts absorption bands, allowing both a clear interpretation of the amide I band and a thicker bulk fluid layer of up to $20\text{ }\mu\text{m}$ [38]. With the exception of studies focused on isotopic exchange, such as deuterated protein or lipid content in D_2O -resilient cells, the resulting red shift in the amide I band [39] and the overall toxic effects of culture viability and biochemistry over time [40–43] render D_2O an unsuitable bulk fluid for drug-cell interaction studies.

In this study, we have tested an in-house water correction algorithm on spectra obtained from different thicknesses of bulk aqueous solution. There is little consensus on an optimum spacer size for IR analysis of living cells, with work published featuring spectra from spacers as small as $4\text{ }\mu\text{m}$ [37] and as large as $20\text{ }\mu\text{m}$ [36]. While the precise effects on cell viability and biochemistry will vary with the natural size of the cell and other factors, it is known that compression of the cell can have an effect on the resulting spectra [35]. This includes variations in the amide I/II peak height ratio and changes in protein and lipid concentrations, which, under severe deformation, can be permanent. Therefore, reducing the compression of the cell as much as possible, without sacrificing spectral quality, is important to maintaining the cell in as close to a natural environment as possible.

The problem of strong water absorption can be overcome through the use of a synchrotron source. The improved quality of spectra, in terms of both spatial and spectral resolution [44] and signal-to-noise ratio [26, 27], is well known, while the increased brightness generated by a synchrotron source relative to a thermal source [45] provides sufficient brilliance of light to penetrate a bulk water layer and still provide a cell spectrum with good signal-to-noise ratio.

Using an in-house water correction algorithm and working with the B22 Multimode Infrared Imaging and Microspectroscopy (MIRIAM) beamline at Diamond Light Source (DLS), we have tested our water correction procedure on hydrated, but chemically fixed, LNCaP prostate cancer cells in 6 and $12\text{ }\mu\text{m}$ spacers to evaluate the effect of pathlength on

resulting biological spectra. Furthermore, we have studied the action of two novel drug treatments on live, hydrated K562 acute myeloid leukaemia (AML) cells with a pathlength that reduces compression of the living cells during analysis.

By using fixed LNCaP cells, in a liquid sample holder, we reduce the potential for biochemical variation between sample replicates, and therefore, differences in spectra should be the result of differences in sample holder loading alone. This gives an indicator of the reproducibility of our method over multiple experiments/replicates.

Meanwhile, poor response rates to conventional chemotherapy and low overall survival rates [46] make AML a focus for new and redeployed therapies [47], especially due to the high toxicity of conventional chemotherapy to older, frailer patients, who make up a significant proportion of sufferers [48].

Colleagues at the University of Salford provided two novel anti-cancer compounds for evaluation of drug-induced biochemical changes at the cellular level: PL63, which is a DNA cross-linking agent and analogue of the commercial anti-cancer drug busulfan [49], and YA1, which is a protein kinase inhibitor [50]. Due to their significantly different modes of action, cells treated with each of these agents should be distinguishable from each other based on their IR spectra and therefore allows us to demonstrate a workflow fit for purpose for FTIR analysis of drug-induced changes at the cellular level in hydrated/living cells.

Methodology

Cell culture

Spacer evaluation LNCaP prostate cancer cells were grown to approximately 90% confluency using RPMI 1640 medium, supplemented with 10 vol.% bovine serum, 1% L-glutamine, 1 mM sodium pyruvate and 10 mM HEPES solution, with 1 µg/ml of puromycin and 2.5 µg/ml of blasticidin antibiotics in T25 culture flasks. Flasks were incubated at 37 °C and 5% CO₂. Cells were harvested using trypsin, washed three times with phosphate-buffered saline (PBS) and fixed in 4% formalin solution.

Novel drug study K562 AML cells were grown in RPMI 1640 medium (+L-glutamine) with 10 vol.% bovine serum and 1 vol.% penicillin-streptomycin at 37 °C and 5% CO₂ in T25 cell culture flasks.

Drug treatment

Novel drug study Twelve to twenty-four hours prior to drug treatment, cells were passaged to ensure they were in exponential growth when the drug was introduced. Flasks were

treated with drug compounds as follows: PL63 was administered at a concentration of 21 nM, equivalent to the IC₅₀ value of busulfan [51], as no reported IC₅₀ specific to PL63 in K562 cells was available; YA1 was administered at the reported IC₅₀ value of 6.2 µM [52]. Solutions of each drug compound were made up in dimethyl sulphoxide (DMSO) such that a dose of 1 µl/ml was added to the culture flask for both treatments; control flasks were administered the equivalent amount of DMSO.

Preparation of cells

Spacer evaluation Formalin-suspended LNCaP cells were centrifuged at 500 g to pellet the cells. The pellet was then washed three times with PBS to remove residual formalin, and the supernatant was discarded after the third wash, leaving the cell pellet in residual PBS. To ensure a suitable concentration of cells for analysis, the measured sample was taken directly from this residual.

Novel drug study Drug-treated and control cells were removed from the incubator and harvested after 1, 10, and 20 h. The sample was centrifuged at 500 g to pellet cells, from which the growth medium was discarded. The pellet was then washed twice with PBS to remove residual medium and any residual extracellular drug. After the second wash, the supernatant was poured away to leave a cell pellet in a residual amount (~0.5 ml) of PBS, from which the measured sample was taken.

Loading of liquid sample holder

Spacer evaluation Samples were measured using 6 and 12 µm spacers in the modified liquid sample holder available on the B22 MIRIAM beamline at Diamond. In each case, an amount of sample slightly less than the calculated volume was pipetted onto a clean 25 mm diameter, 1 mm thick calcium fluoride (CaF₂) window. Using less than the calculated volume prevents completely filling the available space, thereby ensuring a dry area is available for taking a background measurement once the sample holder has been assembled. The sample holder is assembled with o-rings (3 mm) at the base, the CaF₂ slide onto which the spacer and sample are placed, followed by a second CaF₂ slide of the same proportions, and a final o-ring (1 mm). This configuration ensures that pressure is evenly distributed across the holder.

Novel drug study Samples were measured using a 10 µm spacer in the modified liquid sample holder available on the B22 MIRIAM beamline at Diamond. Cell sample (1.5 µl) was pipetted onto a clean CaF₂ window of 25 mm diameter and 1 mm thickness. The sample holder was then assembled in the same configuration as described above.

SR-FTIR measurements

For both studies, data were acquired in transmission using the $\times 36$ objective/condenser optics on a Hyperion 3000 microscope coupled to a Bruker Vertex 80 FTIR spectrometer at the MIRIAM beamline B22 at DLS, using a liquid nitrogen (LN_2)-cooled mercury-cadmium-telluride (MCT), high-sensitivity $50 \mu\text{m}$ pitch detector and $15 \times 15 \mu\text{m}^2$ slit size at the sample.

Two hundred fifty-six co-added scans (circa 35 s) were used for both background and sample measurements. A dry area of the sample was used for the background scan. A minimum of 65 cells per sample loading were selected for measurement using OPUS 7 software, with a corresponding measurement of the bulk PBS layer taken from a cell-free area adjacent to each selected cell for use in water correction. This gave a minimum of 130 spectra in each measurement and equates to approximately 90 min measuring time for optimal spectral quality.

FTIR data processing

Spacer evaluation The spectral contribution of the bulk aqueous solution must be removed before any other processing or analysis of the data can be carried out. This is done with an in-house MATLAB-based water correction algorithm, which performs a least-squares fit of the $1500\text{--}1700 \text{ cm}^{-1}$ range of the sample spectrum to a Matrigel reference. This is used to determine a coefficient by which the corresponding PBS spectrum is multiplied to give the ‘water to be removed (TBR)’, taking account of the different quantities of aqueous solution

present in the cell and PBS spectra. The water TBR spectrum was then subtracted.

The water-corrected LNCaP spectra were then quality controlled, smoothed using a Savitzky-Golay filter with nine points of smoothing and vector normalised. Note that the close refractive index matching of the CaF_2 , water and cell means that reflection artefacts are minimised in the FTIR spectra and resonant Mie scattering from the cell is very much reduced compared with fixed, dried samples. As such, RMieS correction is not required [53–55].

Novel drug study Following water correction, data were quality controlled, vector normalised, converted to the second derivative and then smoothed using a Savitzky-Golay filter, using a third-order polynomial with 13 smoothing points.

The effects of saturation of the water bending mode were observed in the amide I region of a number of spectra with thicker spacers. For simplicity, it was decided to remove this region from all of the spectra. The second derivative spectra were cut to the $1100\text{--}1575$ and $2750\text{--}3000 \text{ cm}^{-1}$ wavenumber regions; this removes the saturated water region, the region below 1100 which is noisy due to the low wavenumber cut-off resulting from the use of 2 mm equivalent CaF_2 thick material, and the $1800\text{--}2800 \text{ cm}^{-1}$ range which contains no biochemical information.

Spectral analysis

Spacer evaluation Mean spectra were computed for each loading in the 6 and $12 \mu\text{m}$ spacers. These were investigated for

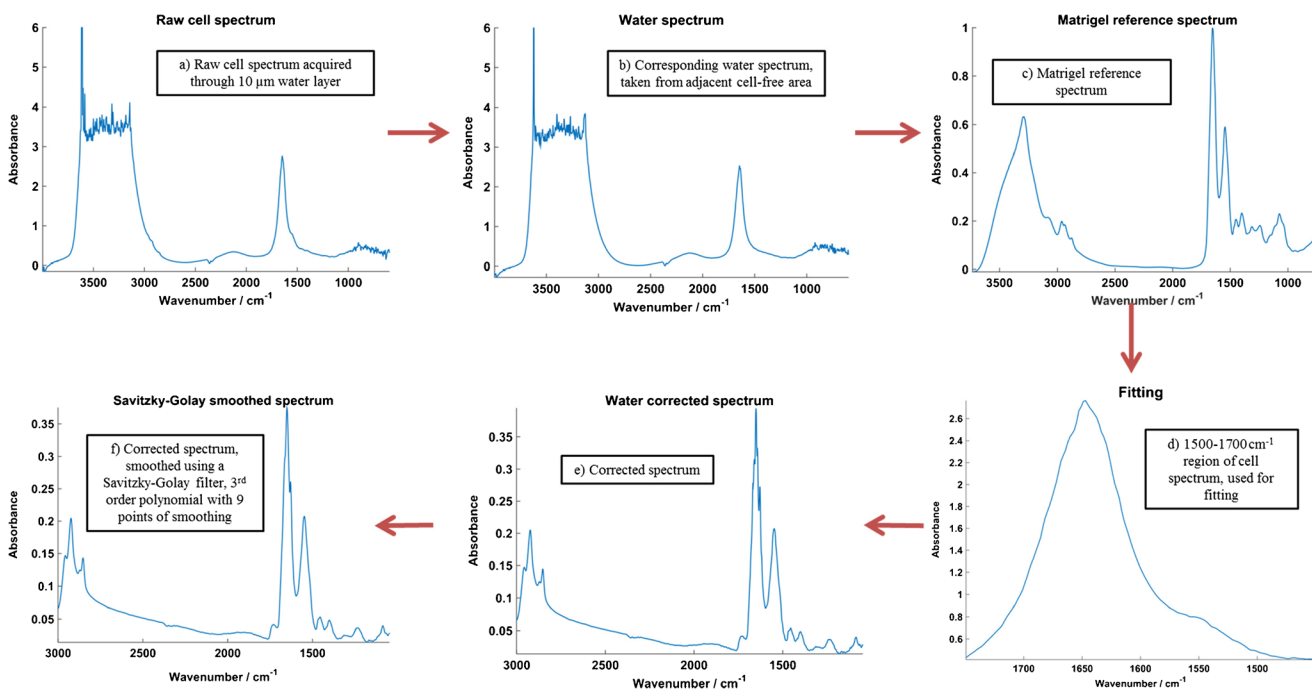


Fig. 1 Schematic to show data processing workflow for the water correction algorithm

variations in peak height, position, shape and any noticeable baseline variations between each of the three replicate loadings using each spacer.

Novel drug study After conversion to the second derivative, mean spectra were computed for each drug treatment and sampling time point. These were investigated for variations in protein, lipid and nucleic acid signatures, both over time (intra-sample) and between different treatments (inter-sample) at the same time point. The data were also analysed using canonical variate analysis (CVA) [56], retaining 21 principal components (PCs), equivalent to 95% of the variation in the lower wavenumber region of the second derivative spectra. Similar methodology, retaining 95% of the variance, has previously been employed for the classification of FTIR and Raman spectra [57, 58]. Fivefold cross-validation was applied to the spectra of control and drug-treated cells; this involves the dataset being split into five groups, with four used for training a classification model and the fifth then projected in as a test dataset. This is repeated five times, with each group acting as the test set once.

Results and discussion

Evaluation of spacer thickness for the analysis of single cells in an aqueous environment

Development of our in-house water correction procedure involved testing on a range of cell types and experimental setups, as well as testing with a number of fitting ranges in order to optimise the procedure. Figure 1 shows a simplified schematic of the correction procedure using a single SR-FTIR example spectrum of a LNCaP cell.

The effectiveness of this in-house procedure on the spectra of formalin-fixed LNCaP cells, which were suspended in PBS and measured using both 6 and 12 μm spacers using SR-FTIR, is subsequently demonstrated. Figure 2 shows mean spectra for each loading of LNCaP cells using the 6 μm (Fig. 2a) and 12 μm (Fig. 2b) spacers. Firstly, this demonstrates the ability of our water correction procedure to extract good quality IR spectra from a water layer approaching the saturation limit, allowing us to reduce the compressive stresses on the cells by operating with a larger spacer.

The mean spectra from the 12 μm spacer show excellent reproducibility across the 2800–3000 cm^{-1} lipid region, consistent peak heights and positions across the amide I and II peaks and also show good consistency throughout the fingerprint region. There is some variation in the replicates in the lower wavenumbers of the fingerprint region, but the overall consistency and reproducibility of the spectra are consistent with the 6 μm repeat loadings, despite the significantly increased water contribution. Key cellular features have also

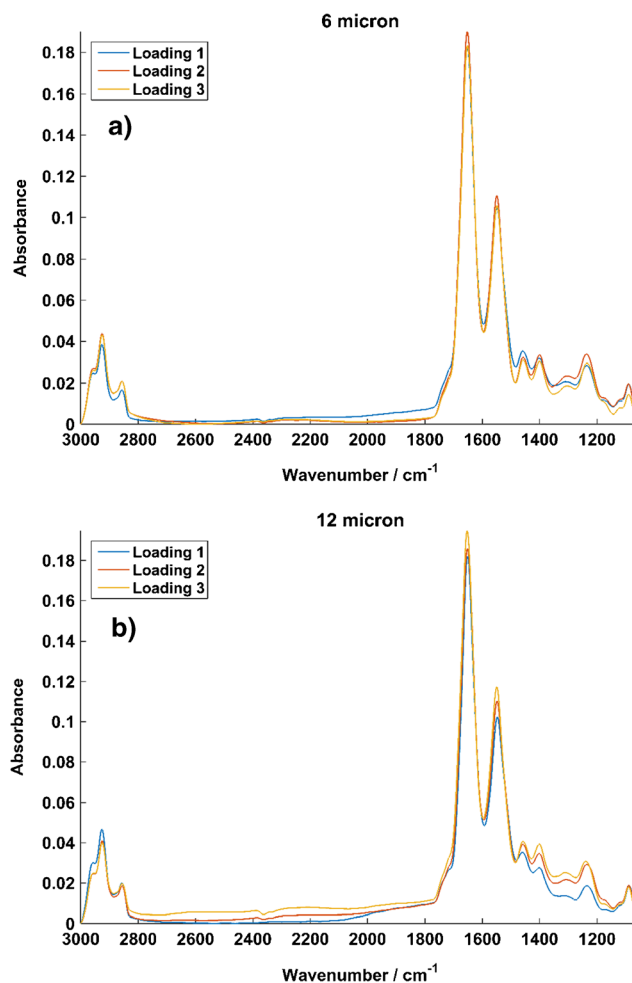


Fig. 2 Vector-normalised mean spectra of 65 LNCaP cells from three repeat loadings of (a) a 6 μm spacer and (b) a 12 μm spacer. The 12 μm loadings show comparable quality and reproducibility, despite the significantly increased water contribution to be removed

been retained throughout the spectrum, despite measurements being taken at close to the water saturation limit.

Observation of novel chemotherapeutic drug modes of action in hydrated cells at the single cell level

Having developed a water correction procedure and sample loading conditions that are able to consistently retain important spectral features, as demonstrated by Fig. 2, the next stage of our study is to test the algorithm on a live cell system. We selected two novel chemotherapy agents, PL63 and YA1, and monitored their effect on live K562 AML cells after 1 and 20 h of treatment.

Having determined through our analysis of spacer thicknesses that good-quality spectra could be obtained at a pathlength above 10 μm , the K562 cells were measured using a 10 μm spacer to reduce the risk of cell movement during measurement. This is due to the slight difference in the average size of LNCaP cells compared to K562; LNCaP cells have

been observed to be up to 20 μm in diameter [59], while K562 cells are generally 15 μm in diameter [60].

Figure 3 shows normalised mean spectra of PL63-treated cells after 1 and 20 h, and DMSO control and drug-treated spectra after 20 h (Fig. 3a, b), along with the second derivative of each (Fig. 3c, d).

Examination of Fig. 3a, b shows no obvious regions of difference between the spectra, either over time or between the control and drug-treated spectra after 20 h. Conversion to the second derivative to enhance spectral features, however, removes any remaining baseline variations and highlights some more interesting biochemical changes. In Fig. 3c, the second derivative spectra are consistent across the majority of the range, apart from in the 1170–1250 cm^{-1} wavenumber range, where the signal from the 20 h spectrum is more intense than at 1 h. This region contains a number of features, including the amide III region and other proteins, but the two strongest signatures, at 1217 and 1244 cm^{-1} , relate to phosphate stretching in DNA and RNA. This is of particular interest, as

PL63 and busulfan—the commercial drug from which it is derived—are known DNA cross-linkers. These differences occurring in the mean spectra over time appear to be directly linked to the mode of action of the agent.

In Fig. 3d, the variations between the control and drug-treated mean spectra are more varied across the spectrum, with greater variation in some of the protein bands than in Fig. 3c, but the specific variations in the phosphate DNA/RNA peaks can still be seen, again linking these variations to the action of the drug.

Figure 4 shows the mean spectra of YA1-treated cells after 1 and 20 h (Fig. 4a), alongside the mean spectra of DMSO-treated control cells and YA1-treated cells after 20 h (Fig. 4b), with the corresponding second derivative spectra shown below (Fig. 4c, d).

The underivatized spectra do not show signs of obvious biochemical differences; the variations in the spectra in Fig. 4a, b could be attributed to baseline variations. However, in the second derivative spectra in Fig. 4c, d,

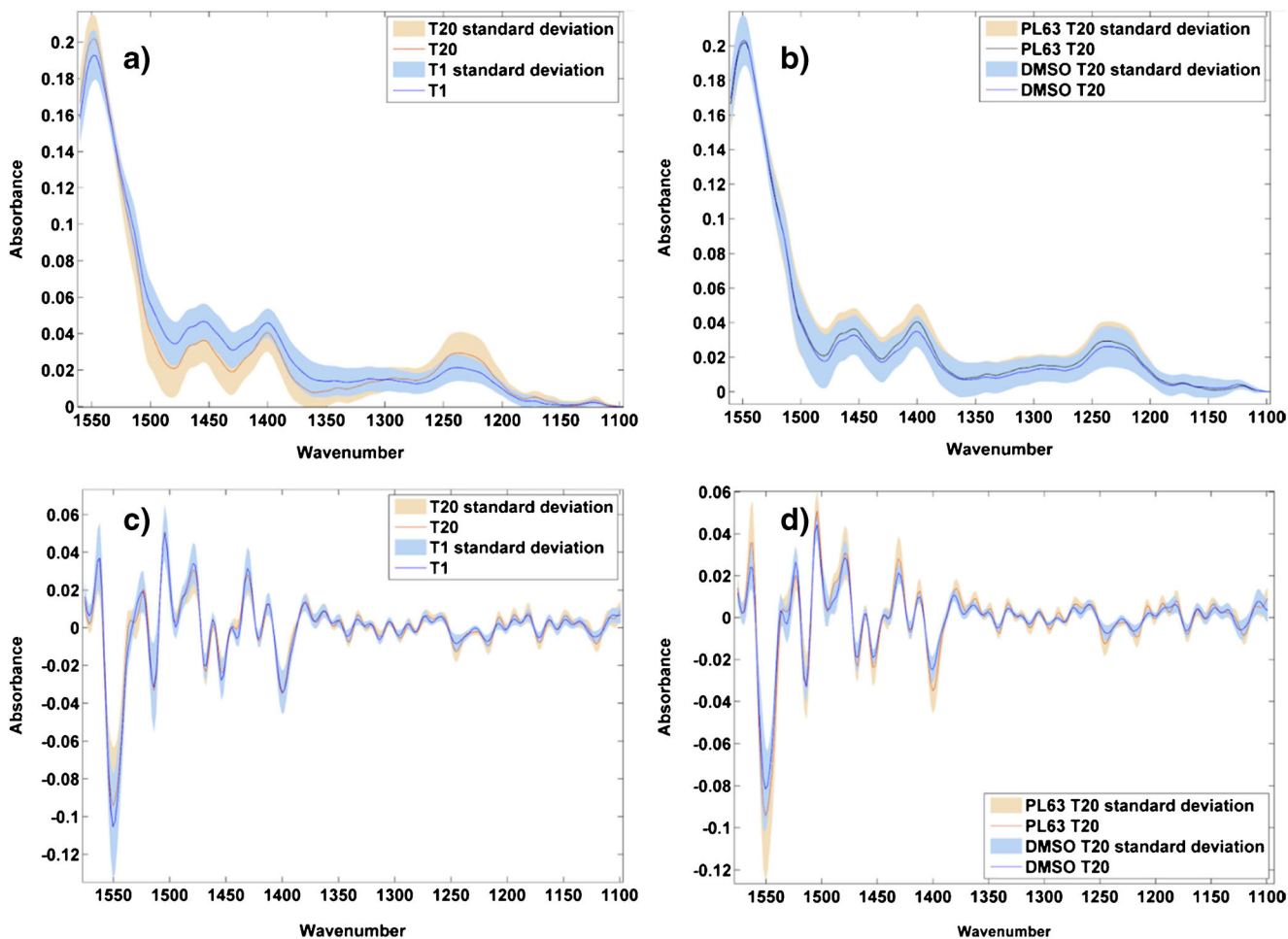


Fig. 3 Normalised mean spectra of 120 cells, from three replicates, overlaid for PL63-treated cells after 1 and 20 h of drug treatment (a) and after 20 h of incubation with DMSO and drug (b). The corresponding

second derivative spectra are shown in (c) and (d) to enhance spectral features corresponding to biological changes with drug treatment. The standard deviation of each mean spectrum is shown by the shaded area

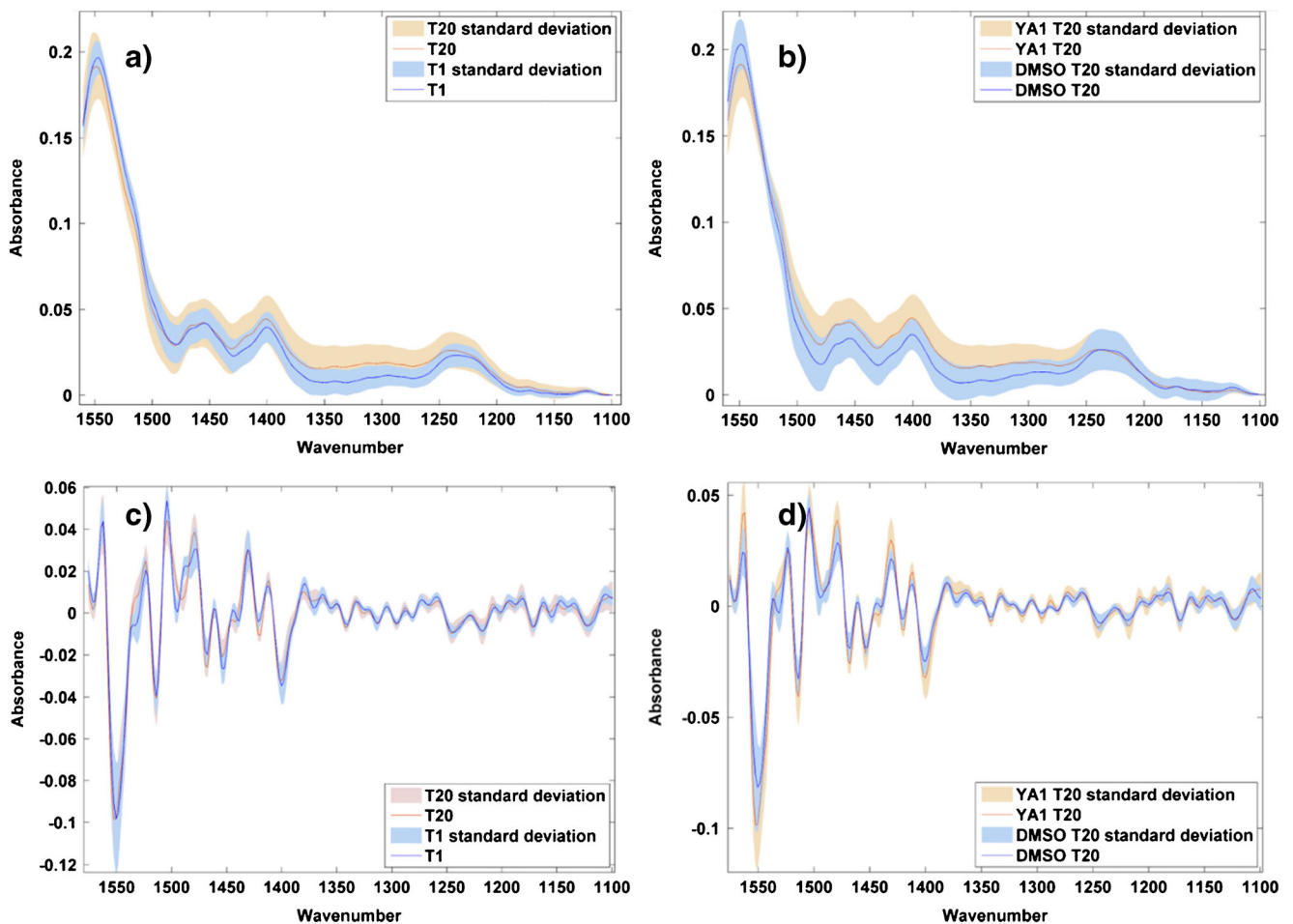


Fig. 4 Normalised mean spectra of 120 cells, from three replicates, overlaid for YA1-treated cells after 1 and 20 h of drug treatment (a) and after 20 h of incubation with DMSO and drug (b). The corresponding

second derivative spectra are shown in (c) and (d) to enhance spectral features corresponding to biological changes with drug treatment. The standard deviation of each spectrum is shown by the shaded area

differences again become more apparent. Significantly, the variations in the DNA/RNA bands noted in the PL63-treated cells are less pronounced, particularly in Fig. 4c when compared to Fig. 3c. The variations in Fig. 4c, d are less specific than those in the PL63-treated spectra but do include the amide II region at $1480\text{--}1560\text{ cm}^{-1}$. This is significant, given that YA1 is known to be a protein kinase inhibitor and would therefore be expected to induce changes in protein structure.

Figures 5 and 6 show the second derivative mean spectra of PL63- and YA1-treated cells, respectively, after 1 and 20 h of treatment, enlarged to the particular region of interest in each case—the phosphate and DNA/RNA bands in Fig. 5 and the amide II region in Fig. 6. The variations in mean spectra over time can be clearly seen in these enlarged images. Of particular interest is the variation in Fig. 5 of the spectra of PL63-treated cells at 1217 and 1244 cm^{-1} , which corresponds with variations in DNA which would not be accessible if studying dehydrated cells.

CVA was employed to assess differences in the response to the K562 cells to each drug. Figure 7 shows a CVA score plot,

retaining 21 PCs, comparing spectra from control, PL63-treated cells, and YA1-treated cells after 20 h. Examination

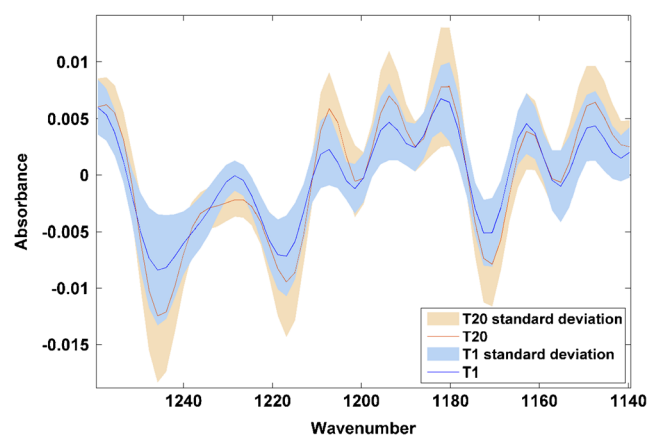


Fig. 5 Enlarged region of mean spectra overlaid for PL63-treated cells after 1 and 20 h of drug treatment. Apparent drug-induced changes can be observed particularly at 1217 and 1244 cm^{-1} as well as from 1180 to 1210 cm^{-1}

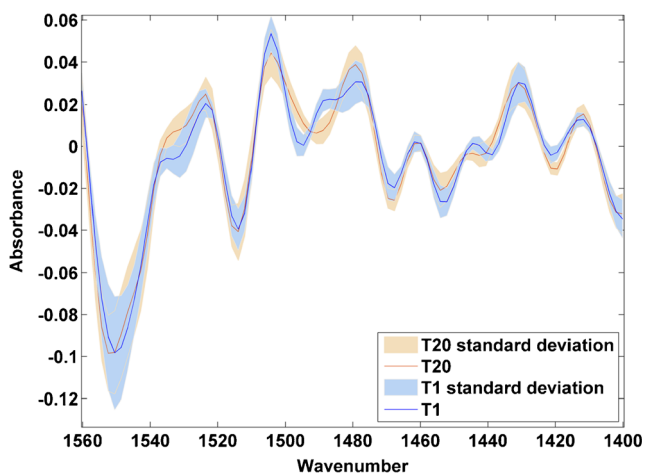


Fig. 6 Enlarged region of mean spectra overlaid for YA1-treated cells after 1 and 20 h of drug treatment. Apparent drug-induced changes can be observed across the 1480–1560 cm^{-1} range, covering the amide II region

of the score plot shows discrimination between control and drug-treated cells across CV1, with grouping evident between the drug-treated classes across CV2. Spectra from 120 individual cells, from three combined replicates, were used in each class.

Multivariate analysis therefore demonstrates that the biochemical changes observed at the single cell level from each of the novel compounds tested can be classified in IR spectra relative to a control. Crucially, it is clearly demonstrated that cells treated with each compound can be distinguished from each other. This is strongest indication that our live, hydrated cell system, with in-house water correction and using a 10 μm spacer, is able to differentiate between the modes of action of novel chemotherapy agents.

Fig. 7 CVA score plot describing 95% of the variance of the second derivative data, showing grouping of DMSO-treated control cells (black) and cells treated with PL63 and YA1 (blue and red, respectively) after 20 h of incubation time

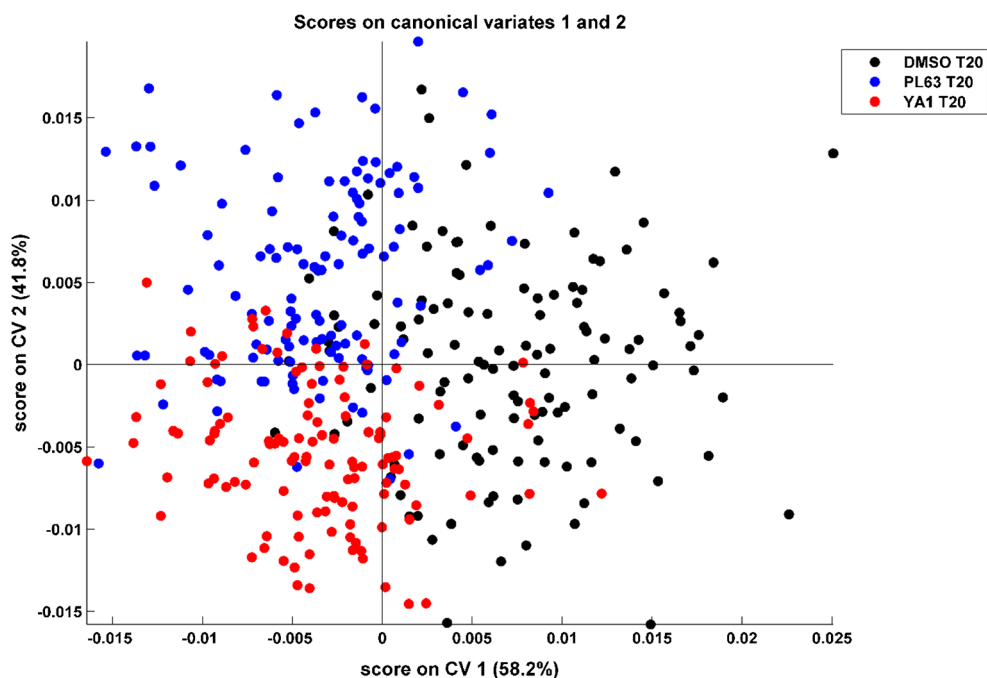


Table 1 Summary of percentage of test spectra correctly classified using k -fold cross-validation of second derivative spectra in the low wavenumber region, showing averages of 80% or greater correctly classified for each group

k	% correctly classified		
	DMSO T20	PL63 T20	YA1 T20
1	79	88	83
2	83	79	79
3	88	88	83
4	75	88	79
5	75	75	79
Range (%)	75–88	75–88	79–83
Mean (%)	80	84	81

To further investigate the observed grouping in the CVA score plot, a fivefold cross-validation was performed on the data. The percentage of correctly classified spectra of each class, for each of the five folds, is shown in Table 1.

Consistent with the score plot shown in Figure 7, fivefold cross-validation clearly shows the ability of SR-FTIR to distinguish between control and drug-treated cell spectra and also between cells treated with compounds with different modes of action. Fivefold cross-validation is able to correctly identify between 75 and 88% of control cells, 75–88% of PL63-treated cells, and 79–83% of YA1-treated cells. This is based on a relatively small sample size of 120 cells per class, giving five test sets of 24 spectra for each of the three classes, but clearly demonstrates clear spectral differences between control cells and cells undergoing different drug treatments. Given that all

three sets of samples have been exposed to DMSO, some degree of similarity in the spectra is to be expected. By using effective water correction and then using the second derivative to highlight small variations in the spectra, we are able to observe spectral differences as a result of the exposure to different novel compounds. This is a promising development in our live cell methodology and demonstrates an ability to gain insight into the effectiveness and mode of action of novel compounds in living cells.

Conclusions

This study has demonstrated an experimental protocol and water correction procedure that is able to obtain high-quality IR spectra from cells in a relatively thick aqueous layer, offering a significant improvement on many reported sample thicknesses for similar studies.

The key measure of any water correction is its ability to retain relatively subtle spectral changes between spectra. With our live cell study of K562 AML cells, we have been able to observe spectral changes in the second derivative between control and drug-treated cells, which can be directly related to the mode of action of that particular drug. Crucially, we have been able to observe differences in drug-treated spectra over time in spectral regions that would not have been observable if using dehydrated cells. For live cell analysis to continue to develop, a more in-depth level of analysis must be available when compared to fixed cells, to compensate for increased experimental complexity.

This experiment is the first employing our new protocol for hydrated cell studies using FTIR, developed in collaboration with the MIRIAM beamline at DLS. Future experiments will expand the range and type of cells investigated using the methodology.

Live cell analysis using SR-FTIR offers the ability to gain new insights into cell behaviour that cannot be obtained from fixed cells, despite the increased experimental complexity. Reducing the physical stress on cells is a significant step towards measurements in close to in vivo conditions as possible, thereby providing more reliable data for understanding drug-induced biochemical changes at a cellular level.

We have also been able to demonstrate the effectiveness of two novel anti-cancer agents on a particularly aggressive cancer type. This indicates, once again, the ability of FTIR to assess drug effectiveness and mode of action.

Acknowledgements LNCaP cells were provided by M. Brown and C. Hart of the Institute for Cancer Science at the University of Manchester. K562 cells were originally kindly donated by A. Southam at the University of Birmingham and subsequently stored at the University of Manchester in the Lockyer group. J. Doherty also acknowledges DLS and UoM for a PhD scholarship. J. Hadfield and colleagues at the University of Salford are acknowledged for providing the agents for the K562 AML study, as is A. Henderson for help with data analysis code. Thanks to all the team at the B22 MIRIAM beamline at DLS, particularly M. Wolna, A. Fitzpatrick and Q. Nguyen for in-house beamtime support.

Funding information P. Gardner and J. Denbigh acknowledge the funding from Diamond Light Source (DLS) for beamtimes SM15375-1 and SM17811-1.

Compliance with ethical standards

Conflict of interest The authors declare that they have no conflict of interest.

Open Access This article is distributed under the terms of the Creative Commons Attribution 4.0 International License (<http://creativecommons.org/licenses/by/4.0/>), which permits unrestricted use, distribution, and reproduction in any medium, provided you give appropriate credit to the original author(s) and the source, provide a link to the Creative Commons license, and indicate if changes were made.

References

- Baker MJ, Gazi E, Brown MD, Shanks JH, Gardner P, Clarke NW. FTIR-based spectroscopic analysis in the identification of clinically aggressive prostate cancer. *Br J Cancer*. 2008;99(11):1859–66.
- Bhargava R. Towards a practical Fourier transform infrared chemical imaging protocol for cancer histopathology. *Anal Bioanal Chem*. 2007;389(4):1155–69.
- Bird B, Romeo MJ, Diem M, Bedrossian K, Laver N, Naber S. Cytology by infrared micro-spectroscopy: automatic distinction of cell types in urinary cytology. *Vib Spectrosc*. 2008;48(1):101–6.
- Gazi E, Baker M, Dwyer J, Lockyer NP, Gardner P, Shanks JH, et al. A correlation of FTIR spectra derived from prostate cancer biopsies with Gleason grade and tumour stage. *Eur Urol*. 2006;50(4):750–61.
- Gazi E, Dwyer J, Gardner P, Ghanbari-Siahkali A, Wade A, Miyan J, et al. Applications of Fourier transform infrared microspectroscopy in studies of benign prostate and prostate cancer. A pilot study. *J Pathol*. 2003;201(1):99–108.
- Mantsch HH. The road to medical vibrational spectroscopy—a history. *Analyst*. 2013;138(14):3863–70.
- Doherty J, Cinque G, Gardner P. Single-cell analysis using Fourier transform infrared microspectroscopy. *Appl Spectrosc Rev*. 2017;52(6):560–87.
- Bellisola G, Cinque G, Vezzalini M, Moratti E, Silvestri G, Redaelli S, et al. Rapid recognition of drug-resistance/sensitivity in leukemic cells by Fourier transform infrared microspectroscopy and unsupervised hierarchical cluster analysis. *Analyst*. 2013;138(14):3934–45.
- Bellisola G, Della Peruta M, Vezzalini M, Moratti E, Vaccari L, Birarda G, et al. Tracking InfraRed signatures of drugs in cancer cells by Fourier transform microspectroscopy. *Analyst*. 2010;135(12):3077–86. <https://doi.org/10.1039/c0an00509f>.
- Flower KR, Khalifa I, Bassan P, Démoulin D, Jackson E, Lockyer NP, et al. Synchrotron FTIR analysis of drug treated ovarian A2780 cells: an ability to differentiate cell response to different drugs? *Analyst*. 2011;136(3):498–507.
- de Carvalho AB, Pilling M, Gardner P, Doherty J, Cinque G, Wehbe K, et al. Chemotherapeutic response to cisplatin-like drugs in human breast cancer cells probed by vibrational microspectroscopy. *Faraday Discuss*. 2016;187:273–98.
- Denbigh JL, Perez-Guaita D, Vernooij RR, Tobin MJ, Bamberg KR, Xu Y, et al. Probing the action of a novel anti-leukaemic drug therapy at the single cell level using modern vibrational spectroscopy techniques. *Sci Rep*. 2017;7:2649.
- Hughes C, Brown M, Clarke N, Flower K, Gardner P. Investigating cellular responses to novel chemotherapeutics in renal cell carcinoma using SR-FTIR spectroscopy. *Analyst*. 2012;137(20):4720–6.

14. Hughes C, Brown M, Ball F, Monjardez G, Clarke N, Flower K, et al. Highlighting a need to distinguish cell cycle signatures from cellular responses to chemotherapeutics in SR-FTIR spectroscopy. *Analyst*. 2012;137(24):5736–42.
15. Jimenez-Hernandez M, Brown MD, Hughes C, Clarke NW, Gardner P. Characterising cytotoxic agent action as a function of the cell cycle using fourier transform infrared microspectroscopy. *Analyst*. 2015;140(13):4453–64.
16. Gazi E, Dwyer J, Lockyer NP, Miyan J, Gardner P, Hart C, et al. Fixation protocols for subcellular imaging by synchrotron-based Fourier transform infrared microspectroscopy. *Biopolymers*. 2005;77(1):18–30.
17. Lyng FM, Gazi E, Gardner P. Preparation of tissues and cells for infrared and Raman spectroscopy and imaging. 2011.
18. Vaccari L, Birarda G, Businaro L, Pacor S, Greci G. Infrared microspectroscopy of live cells in microfluidic devices (MD-IRMS): toward a powerful label-free cell-based assay. *Anal Chem*. 2012;84(11):4768–75. <https://doi.org/10.1021/ac300313x>.
19. Pevsner A, Diem M. Infrared spectroscopic studies of major cellular components. Part I: the effect of hydration on the spectra of proteins. *Appl Spectrosc*. 2001;55(6):788–93.
20. Pevsner A, Diem M. Infrared spectroscopic studies of major cellular components. Part II: the effect of hydration on the spectra of nucleic acids. *Appl Spectrosc*. 2001;55(11):1502–5.
21. Pevsner A, Diem M. IR spectroscopic studies of major cellular components. III. Hydration of protein, nucleic acid, and phospholipid films. *Biopolymers*. 2003;72(4):282–9.
22. Wood BR. The importance of hydration and DNA conformation in interpreting infrared spectra of cells and tissues. *Chem Soc Rev*. 2016;45(7):1980–98.
23. Whelan DR, Bambery KR, Heraud P, Tobin MJ, Diem M, McNaughton D, et al. Monitoring the reversible B to A-like transition of DNA in eukaryotic cells using Fourier transform infrared spectroscopy. *Nucleic Acids Res*. 2011;39(13):5439–48.
24. Bentley AJ, Nakamura T, Hammiche A, Pollock HM, Martin FL, Kinoshita S, et al. Characterization of human corneal stem cells by synchrotron infrared micro-spectroscopy. *Mol Vis*. 2007;13:237.
25. Quaroni L, Zlateva T, Normand E. Detection of weak absorption changes from molecular events in time-resolved FT-IR spectromicroscopy measurements of single functional cells. *Anal Chem*. 2011;83(19):7371–80.
26. Holman H-YN, Bechtel HA, Hao Z, Martin MC. Synchrotron IR spectromicroscopy: chemistry of living cells. *Anal Chem*. 2010;82(21):8757–65. <https://doi.org/10.1021/ac100991d>.
27. Holman H-YN, Hao Z, Martin MC, Bechtel HA. Infrared spectromicroscopy: probing live cellular responses to environmental changes. *Synchrotron Radiat News*. 2010;23(5):12–9. <https://doi.org/10.1080/08940886.2010.516737>.
28. Cinque G, Frogley MD, Wehbe K, Nguyen T-NQ, Fitzpatrick A, Kelley CS. Synchrotron-based infrared spectral imaging at the MIRIAM beamline of diamond light source. *Synchrotron Radiat News*. 2017;30(4):11–6.
29. Dong A, Huang P, Caughey WS. Protein secondary structures in water from second-derivative amide I infrared spectra. *Biochemistry*. 1990;29(13):3303–8.
30. Marcsisin EJ, Uttero CM, Miljkovic M, Diem M. Infrared microspectroscopy of live cells in aqueous media. *Analyst*. 2010;135(12):3227–32. <https://doi.org/10.1039/c0an00548g>.
31. Movasaghi Z, Rehman S, ur Rehman DI. Fourier transform infrared (FTIR) spectroscopy of biological tissues. *Appl Spectrosc Rev*. 2008;43(2):134–79.
32. Mourant JR, Gibson RR, Johnson TM, Carpenter S, Short KW, Yamada YR, et al. Methods for measuring the infrared spectra of biological cells. *Phys Med Biol*. 2003;48(2):243.
33. Moss DA, Keese M, Pepperkok R. IR microspectroscopy of live cells. *Vib Spectrosc*. 2005;38(1):185–91.
34. Alberts B, Johnson A, Lewis J, Raff M, Roberts K, Walter P. *Molecular biology of the cell*. New York: Garland Science; 2002.
35. Birarda G, Greci G, Businaro L, Marmioli B, Pacor S, Piccirilli F, et al. Infrared microspectroscopy of biochemical response of living cells in microfabricated devices. *Vib Spectrosc*. 2010;53(1):6–11.
36. Quaroni L, Zlateva T, Wehbe K, Cinque G. Infrared imaging of small molecules in living cells: from in vitro metabolic analysis to cytopathology. *Faraday Discuss*. 2016;187:259–71.
37. Gelfand P, Smith RJ, Stavitski E, Borchelt DR, Miller LM. Characterization of protein structural changes in living cells using time-lapsed FTIR imaging. *Anal Chem*. 2015.
38. Paul J, Provencal R, Saykally R. Characterization of the (D2O) 2 hydrogen-bond-acceptor antisymmetric stretch by IR cavity ringdown laser absorption spectroscopy. *J Phys Chem A*. 1998;102(19):3279–83.
39. Quaroni L, Zlateva T, Sarafimov B, Kreuzer HW, Wehbe K, Hegg EL, et al. Synchrotron based infrared imaging and spectroscopy via focal plane array on live fibroblasts in D 2 O enriched medium. *Biophys Chem*. 2014;189:40–8.
40. Carr G, Miller L, Dumas P. Synchrotron radiation as a source for infrared microspectroscopic imaging with 2D multi-element detection biomedical applications of synchrotron infrared microspectroscopy vol 11 ed D Moss. Royal Society of Chemistry; 2011.
41. Cioni P, Strambini GB. Effect of heavy water on protein flexibility. *Biophys J*. 2002;82(6):3246–53.
42. Hohlefeldt LS, Stögbauer T, Opitz M, Bayerl TM, Rädler JO. Heavy water reduces GFP expression in prokaryotic cell-free assays at the translation level while stimulating its transcription. *Biomed Res Int*. 2013; 2013.
43. Manson LA, Carp RI, Defendi V, Rothstein EL, Hartzell RW, Kritchevsky D. The effect of deuterium oxide on virus-host interaction. *Ann N Y Acad Sci*. 1960;84(16):685–94.
44. Carr GL, Chubar O, Dumas P. Multichannel detection with a synchrotron light source: design and potential. *Spectrochemical analysis using infrared multichannel detectors*. Hoboken: Blackwell Publishing Ltd; 2007. p. 56–84.
45. Dumas P, Sockalingum GD, Sule-Suso J. Adding synchrotron radiation to infrared microspectroscopy: what's new in biomedical applications? *Trends Biotechnol*. 2007;25(1):40–4.
46. Peloquin GL, Chen Y-B, Fathi AT. The evolving landscape in the therapy of acute myeloid leukemia. *Protein Cell*. 2013;4(10):735–46.
47. Ashburn TT, Thor KB. Drug repositioning: identifying and developing new uses for existing drugs. *Nat Rev Drug Discov*. 2004;3(8):673.
48. Büchner T, Berdel WE, Haferlach C, Haferlach T, Schnittger S, Müller-Tidow C, et al. Age-related risk profile and chemotherapy dose response in acute myeloid leukemia: a study by the German Acute Myeloid Leukemia Cooperative Group. *J Clin Oncol*. 2009;27(1):61–9.
49. Westerhof GR, Ploemacher RE, Boudewijn A, Blokland I, Dillingh JH, McGown AT, et al. Comparison of different busulfan analogues for depletion of hematopoietic stem cells and promotion of donor-type chimerism in murine bone marrow transplant recipients. *Cancer Res*. 2000;60(19):5470–8.
50. Hampson L, He X, Oliver A, Hadfield J, Kemp T, Butler J, et al. Analogues of Y27632 increase gap junction communication and suppress the formation of transformed NIH3T3 colonies. *Br J Cancer*. 2009;101(5):829.
51. Czyzewski K, Styczynski J. Imatinib is a substrate for various multidrug resistance proteins. *Neoplasma*. 2009;56(3):202.
52. Kemp T. *Synthesis and evaluation of novel kinase inhibitors as anti-cancer agents*. Salford: University of Salford; 2012.
53. Bassan P, Byrne HJ, Bonnier F, Lee J, Dumas P, Gardner P. Resonant Mie scattering in infrared spectroscopy of biological

- materials—understanding the ‘dispersion artefact’. *Analyst*. 2009;134(8):1586–93.
54. Bassan P, Kohler A, Martens H, Lee J, Byrne HJ, Dumas P, et al. Resonant Mie scattering (RMieS) correction of infrared spectra from highly scattering biological samples. *Analyst*. 2010;135(2):268–77. <https://doi.org/10.1039/b921056c>.
55. Bassan P, Kohler A, Martens H, Lee J, Jackson E, Lockyer N, et al. RMieS-EMSC correction for infrared spectra of biological cells: extension using full Mie theory and GPU computing. *J Biophotonics*. 2010;3(8–9):609–20.
56. Nørgaard L, Bro R, Westad F, Engelsen SB. A modification of canonical variates analysis to handle highly collinear multivariate data. *J Chemom*. 2006;20(8–10):425–35.
57. Crow P, Barrass B, Kendall C, Hart-Prieto M, Wright M, Persad R, et al. The use of Raman spectroscopy to differentiate between different prostatic adenocarcinoma cell lines. *Br J Cancer*. 2005;92(12):2166.
58. Harvey T, Gazi E, Henderson A, Snook R, Clarke N, Brown M, et al. Factors influencing the discrimination and classification of prostate cancer cell lines by FTIR microspectroscopy. *Analyst*. 2009;134(6):1083–91.
59. Song H, Lacks DJ, Enmon RM, Jain SK. Monte Carlo simulation of LNCaP human prostate cancer cell aggregation in liquid-overlay culture. *Biotechnol Prog*. 2003;19(6):1742–9.
60. Kang G, Kim Y-J, Moon H-S, Lee J-W, Yoo T-K, Park K, et al. Discrimination between the human prostate normal cell and cancer cell by using a novel electrical impedance spectroscopy controlling the cross-sectional area of a microfluidic channel. *Biomicrofluidics*. 2013;7(4):044126.